Food Bioscience 61 (2024) 104577

Contents lists available at ScienceDirect

Food Bioscience

journal homepage: www.elsevier.com/locate/fbio

Colorimetric sensing based on silver nanoparticle-functionalized copper porphyrin nanozyme for glyphosate

Li-Hong Yu, Rui Jiang, Cheng-Lin Yang, Yue-Hong Pang, Xiao-Fang Shen [*]

School of Food Science and Technology, Jiangnan University, Wuxi, 214122, People's Republic of China

ARTICLE INFO

Keywords:
Glyphosate
Metal organic framework
Copper porphyrin
Nanozyme
Colorimetric sensor

ABSTRACT

Glyphosate, a widely used herbicide due to the broad-spectrum and high-efficiency properties, has the potential to accumulate in the human body via agricultural food and water sources throughout the food chain. Its safety for both human health and aquatic ecosystems remains a topic of significant debate. In this study, the presence of glyphosate could be directly detected through a notable colorimetric change in an aqueous solution. For this purpose, a silver nanoparticle-functionalized copper porphyrin metal-organic framework (AgNPs/Cu-TCPP) nanozyme was conveniently prepared for colorimetric sensing of glyphosate. The as-synthesized nanozyme that modified AgNPs with Cu-TCPP metal-organic framework as the precursor, has excellent peroxidase mimetic activity and specific recognition performance of glyphosate. The nanozyme demonstrated the ability to catalyze the oxidation of 3,3,5,5-tetramethylbenzidine (TMB) using H_2O_2, resulting in a marked change in color. When glyphosate was added, which bonded with Cu^{2+}, led to the occupation of the surface-active sites of the nanozyme, thereby making its catalytic performance ineffective. The concentration of glyphosate exhibited a linear range spanning from 2 to 400 μmol L^{-1}, and the limit of detection was 0.67 μmol L^{-1} (S/N = 3). The colorimetric sensing approach employing AgNPs/Cu-TCPP nanozyme exhibits remarkable selectivity and reproducibility, enabling the detection of real samples with recovery rates of 98.3%–103.5%, indicating its potential applicability in safeguarding water and food quality.

1. Introduction

Glyphosate (GLY), a high-efficiency, broad-spectrum, low toxicity and non-selective herbicide, has been widely extensively utilized globally since 1974 (Duke, 2018). Genetically modified crops that are resistant to glyphosate comprise approximately 80% of all such crops, and globally, the annual consumption of glyphosate has surpassed eight hundred thousand tons (Nova et al., 2020). The widespread and excessive use of glyphosate in vast regions has resulted in residual traces being deposited in soil and surface waters, ultimately leading to the accumulation in human bodies via the food chain. Due to the broad application, glyphosate and its possible health implications, including the risk of cancer, have garnered significant attention from both public health and the scientific community (Dallegrave et al., 2003). Until now, the evidence surrounding glyphosate's toxicity and carcinogenicity remains inconclusive (Berry, 2020). It is worth noting that in 2015, the International Agency for Research on Cancer designated glyphosate as a potential (group 2A) carcinogen for humans, based in part on limited epidemiological data linking it to non-Hodgkin lymphoma (Guyton et al., 2015). And the World Health Organization (WHO) limits glyphosate concentrations in drinking water to 0.9 μg mL^{-1} (De Almeida et al., 2015). Therefore, developing a rapid, convenient and efficient GLY detection method is of great significance for the food safety.

Currently, the primary methods for detecting GLY involve high-performance liquid chromatography (Yoshioka et al., 2011), gas chromatography (Wei et al., 2024), and capillary electrophoresis (Graf et al., 2022). Although these methods have high sensitivity and stability, they have the limitations in application due to the expensive equipment, professional instrument operators and lengthy analysis times. Recently, the colorimetric sensing method has been widely used in the detection field because of its high signal-to-noise ratio and easy visualization. Nanozymes are inorganic nanomaterials with enzyme-like activity and have recently attracted significant attention in the field of analysis chemistry. In comparison to nature enzymes, this artificial enzyme has several advantages including high stability, short purification time, and competitive cost (Chang et al., 2023).

Nanozymes with restricted specific surface areas and poor dispersibility present obstacles in efficiently interacting with substrate

---

[*] Corresponding author.
E-mail address: xfshen@jiangnan.edu.cn (X.-F. Shen).

https://doi.org/10.1016/j.fbio.2024.104577
Received 29 April 2024; Received in revised form 3 June 2024; Accepted 13 June 2024

molecules. Recently, nanozymes deriving from metal-organic frameworks (MOFs) have attracted considerable attention from researchers. Their varied surface areas and pore dimensions notably boost nanozyme activity by facilitating the accessibility of substrate molecules to the active sites, thereby addressing certain constraints linked to conventional nanozymes (Farhadi et al., 2021). Li et al. (2019) successfully synthesized a Co-MOF exhibiting peroxide mimic enzyme activity through a hydrothermal method, which can effectively enhance the luminol-H_2O_2 chemiluminescence signal. Wang et al. (2020) reported a Zr-MOF exhibits favorable peroxide mimic enzyme activity duo to its unique dipyridyl-based ligands. However, catalytic activity of single MOFs is often considered insufficient (Zhang et al., 2019), there is still much room for exploration in designing and synthesizing MOFs with high peroxidase mimetic activity and binding specificity.

Noble metal nanoparticles (gold, silver, titanium and platinum, etc.) have intrinsic peroxidase mimetic activity catalytic activity (Liu et al., 2022). Since 2007, Gao et al. (2007) first reported on the peroxidase mimicry activity of ferromagnetic nanoparticles, a series of nanocrystal-like active materials containing transition metal ions (iron (Hu et al., 2014), cobalt (Kirandeep et al., 2019), copper (Li et al., 2013), etc.) have been developed. They are often used for detection of reducing substances because of their effective capability to produce reactive oxygen species (ROS). The modification of MOFs with noble metal nanoparticles could effectively improve peroxidase mimetic activity of composite nanoparticles, which beneficial to the development of colorimetric sensor. However, the recognition function of composite nanozyme still needs to be further improved, which allows the specific binding of GLY to avoid the potential interference from the matrix. Therefore, it is still highly desired to develop a remarkable selective composite nanozyme for determination of GLY. Hence, through the modification of noble metal nanoparticles and the manipulation of central metal atoms in MOFs to facilitate targeted binding with glyphosate, nanozymes can be synthesized with enhanced catalytic activity and selective recognition capabilities.

To implement the aforementioned assumptions, we synthesized a AgNPs/Cu-TCPP nanozyme through typical solvothermal method. AgNPs/Cu-TCPP exhibits a crumpled nanosheet morphology, encompassing a large specific surface area along with an abundance of catalytic active sites, which can further catalyzed H_2O_2 to produce hydroxyl radicals. In the presence of GLY, the catalytic site on the surface of AgNPs/Cu-TCPP nanozyme was occupied by GLY, which decreased the peroxidase mimetic activity, resulting in the reaction system from blue to colorless. The constructed colorimetry sensor showed excellent catalytic activity and selectivity, and was successfully applied in cucumber and water samples.

2. Material and methods

2.1. Reagents and materials

GLY was purchased from Aladdin (Shanghai, China). Organophosphorus pesticides including phosalone, profenofos, parathion, parathion-methyl and phorate were obtained from Maclin Biochemical Technology Co., LTD (Shanghai, China). Tetrakis(4-carboxyphenyl) porphyrin was purchased from Enokay (Beijing, China). TMB was obtained from J&K Chemical (Beijing, China). Polyvinylpyrrolidone, Na_2SO_4, $MgSO_4$, $Cu(NO_3)_2{\cdot}3H_2O$, $ZnCl_2$, Na_2CO_3, $NaHCO_3$, NaAc, HAc, ethanol, N, N-dimethylformamide (DMF), trifluoroacetic acid (CF_3COOH), $AgNO_3$, $NaBH_4$, 30% H_2O_2 were purchased from Sinopharm Reagent Co., LTD (Shanghai, China). Different brands (including Dongting Mountain and Kadila) of drinking water and cucumber were purchased from local supermarkets in Wuxi.

2.2. Instruments

The synthesized nanozyme was thoroughly characterized using various techniques. Its morphological features were examined by a scanning electron microscope (SEM, model SU8100 from Hitachi) and a transmission electron microscope (TEM, model FEI TalosF200x from Thermo Scientific). X-ray diffractometer (XRD, D2 PHASER, Brock AXS) and X-ray photoelectron spectrometer (XPS, K-Alpha, Thermo Scientific), IS10 FTIR spectrometer (Nicolet, USA) were also used to characterize other properties. The catalytic activity of the synthesized nanozyme was investigated by UV–visible spectrophotometer (UV–vis, T9, Beijing General Analysis Instrument Co., LTD). The kinetic analysis of catalytic system and the determination of GLY were studied by a microplate analyzer (Gl124i-Epoch, BioTek).

2.3. Synthesis of AgNPs/Cu-TCPP nanozyme

Firstly, the Cu-TCPP was prepared by solvothermal method (Liu et al., 2021). And then the AgNPs/Cu-TCPP nanozyme was prepared through the direct reduction of $AgNO_3$ using sodium borohydride directly on the MOFs (Ma et al., 2019). 5 mg Cu-TCPP was evenly dispersed in 10 mL distilled water, 1.0 mL $AgNO_3$ solution (2.0 mmol L^{-1}) was mixed by ultrasound, then 0.75 mL fresh sodium borohydride solution (10.0 mmol L^{-1}) was added by dropping while stirring. Finally, AgNPs/Cu-TCPP was obtained by magnetic stirring reaction at room temperature for a duration of 2 h, then centrifugation at 8000 rpm, washed with ethanol twice and dried in oven at 60 °C. for a duration of 2 h.

2.4. Study on catalytic activity of AgNPs/Cu-TCPP nanozyme

To investigate the simulated peroxidase mimetic activity of the AgNPs/Cu-TCPP nanozyme, different materials (Cu-TCPP, AgNPs/Cu-TCPP) and the reaction system with GLY were prepared. The absorption spectrum of the reaction system was measured by UV–vis, and the absorption peak at 650 nm was explored. In addition, the effects of reaction time, buffer pH, substrate TMB concentration, H_2O_2 concentration on GLY inhibition of AgNPs/Cu-TCPP nanozyme reaction were investigated.

2.5. Kinetic analysis

When the concentration of TMB was fixed at 0.5, 1, 2 mmol L^{-1} (or the concentration of H_2O_2 was fixed at 20, 40, 80 mmol L^{-1}), the steady-state kinetics of acetic acid/sodium acetate buffer solution (ABS) was studied in different concentrations of H_2O_2 (or TMB) in pH 6.0 and 0.025 mg mL^{-1} AgNPs/Cu-TCPP. The kinetic parameters are determined by utilizing the Michaelis-Menten equation and constructing a Lineweaver-Burk plot. The specific equation employed for this calculation is as follows (Chen et al., 2018):

$$v = \frac{V_{max} \times [S]}{K_m + [S]}$$

$$\frac{1}{v} = \frac{K_m + [S]}{V_{max} \times [S]} = \frac{K_m}{V_{max}} \times \frac{1}{[S]} + \frac{1}{V_{max}}$$

Where v is the initial velocity, V_{max} denotes the maximum reaction velocity, [S] stands for the concentration of the substrate, and K_m is referred to as the Michaelis constant.

2.6. Colorimetric sensing of GLY

A colorimetric sensing method for GLY was build using inhibition of GLY on the peroxidase mimetic activity of AgNPs/Cu-TCPP nanozyme. 0.025 mg mL^{-1} AgNPs/Cu-TCPP dispersion, 2 mmol L^{-1} TMB, 80 mmol L^{-1} H_2O_2, and different concentrations of GLY were added to 0.1 mol L^{-1}ABS. After reaction for 20 min, the absorbance of the reaction system was measured at a wavelength of 650 nm. The ultra-pure water was added to the catalytic reaction system instead of GLY. The absorbance differences between blank samples and GLY samples ($\Delta A_{650} = \Delta A_{blank}$-$\Delta A_{GLY}$) was used to determine GLY indirectly.

2.7. Selectivity and reproducibility validation

In order to investigate the selectivity of colorimetric sensing reaction system, 50 μmol L^{-1} GLY and 500 μmol L^{-1} possible interference substances were added to AgNPs/Cu-TCPP nanozyme reaction system, respectively. After 20 min, the absorbance difference ΔA_{650} was recorded. The interfering substances added were organophosphorus pesticides (including phosalone, profenofos, parathion, parathion-methyl and phorate), metal ions, and possible metal ions (Mg^{2+}, Na^{+}, Zn^{2+}) and general acid ions (SO_4^{2-}, HCO_3^{-}, CO_3^{2-}, NO_3^{-}).

2.8. Samples preparation for GLY analysis

The colorimetric sensing reaction system was employed for the quantitative determination of GLY in drinking water and cucumber samples. 25 g dried cucumber sample was weighed and placed in a beaker, then water was added to a constant volume of 125 mL. The sample was subjected to ultrasonic treatment for 1 h to ensure thorough mixing and then centrifuged at 3500 rpm for 10 min. 15 mL supernatant was taken to the centrifuge tube, and an equal amount of methylene chloride was added. The mixture was then vortexed for 2 min to ensure thorough mixing, and centrifugated at 3500 rpm for 5 min. 4.5 mL of supernatant was placed in a centrifuge tube, and 0.5 mL ABS (0.1 mol L^{-1}, pH 6) was added. Finally, the samples underwent filtering through a 0.45 μm membrane to eliminate particulate matter and stored at 4 °C for further analysis. Additionally, three different brands of drinking water were also filtered using a 0.45 μm membrane to ensure their purity and suitability for the intended application.

3. Results and discussion

3.1. Design of a colorimetric sensor for GLY based on AgNPs/Cu-TCPP

GLY colorimetric sensor based on AgNPs/Cu-TCPP peroxidase mimetic activity simulation was shown in Fig. 1. AgNPs/Cu-TCPP was able to catalyze the peroxidase substrate TMB into aquamarine blue oxidized TMB (OxTMB). The catalytic activity of AgNPs/Cu-TCPP was inhibited with the addition of GLY, resulting in color gradually changes from aquamarine blue to colorless. This phenomenon can be attributed to the ability of the three donor groups of GLY (carboxylate, amine, phosphate) to establish two pentagonal equatorial planes with Cu^{2+}, resulting in the formation of stable complexes through strong specific interactions (Coutinho et al., 2007). The layered structure of AgNPs/Cu-TCPP with a central metal of Cu^{2+} can provide numerous binding sites, thus allowing AgNPs/Cu-TCPP nanozyme to selectively chelate with GLY, resulting in a severe steric hindrance of electron transfer and a significant decrease in catalytic activity. Based on these outcomes, a novel colorimetric strategy was developed for screening GLY.

3.2. Characterization of nanozyme

The catalytic capacity of nanozyme was closely related to the surface structure (Xu et al., 2019). The SEM image of Cu-TCPP revealed a flower-like morphology constructed from ultra-thin nanosheets, which were evenly shaped and stacked in sheets (Fig. 2A). The unique flower structure of Cu-TCPP provided large adhesion sites for AgNPs binding, and AgNPs were uniformly attached to the Cu-TCPP surface, indicating that AgNPs/Cu-TCPP have been successfully prepared (Fig. 2B). TEM images were used to analyze the morphology and structure characteristics of Cu-TCPP and AgNPs/Cu-TCPP (Fig. S1). Fig. S1A showed the ultrathin sheet structure with some folds on the surface of the nanosheet. Fig. S1B showed the combination of AgNPs and Cu-TCPP. AgNPs was evenly attached to Cu-TCPP, and the pleated structure of Cu-TCPP was still clearly visible.

For crystal structure determination, XRD was utilized to characterize the precursor MOF and AgNPs/Cu-TCPP nanozyme. As depicted in Fig. 2C, the distinct diffraction peak observed at 19.57° corresponds precisely to the (002) crystal plane of Cu-TCPP (Huang et al., 2017). Fig. 2D showed strong reflection peaks at 38.31°, 43.09°, 64.57°, and 77.31°, which could index Ag crystal planes of (111), (200), (220), and (311), proving the successful preparation of AgNPs in the surface of Cu-TCPP (Ma et al., 2019).

The structures of MOFs (Cu-TCPP) and MOFs-derived nanozyme (AgNPs/Cu-TCPP) were investigated using XPS. Fig. 3A is the full XPS spectrum of AgNPs/Cu-TCPP nanozyme, and it is obvious that AgNPs and Cu^{2+} were successfully modified. In the spectra of TCPP shows the peaks at 529.5 (C═O) and 530.7 eV (C–OH) (Fig. 3B). Compared to TCPP, a notable reduction in the O1s peak intensity of C–O was observed in MOFs, with the peak shifting to 531.2 eV, indicating the substitution

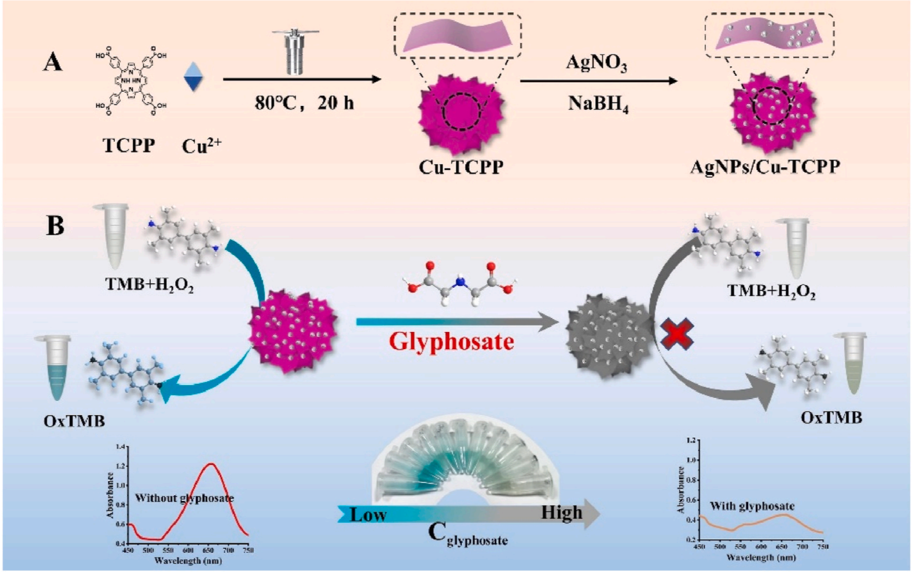

Fig. 1. Colorimetric sensing of GLY based on the strong inhibition of peroxidase mimetic activity of AgNPs/Cu-TCPP.

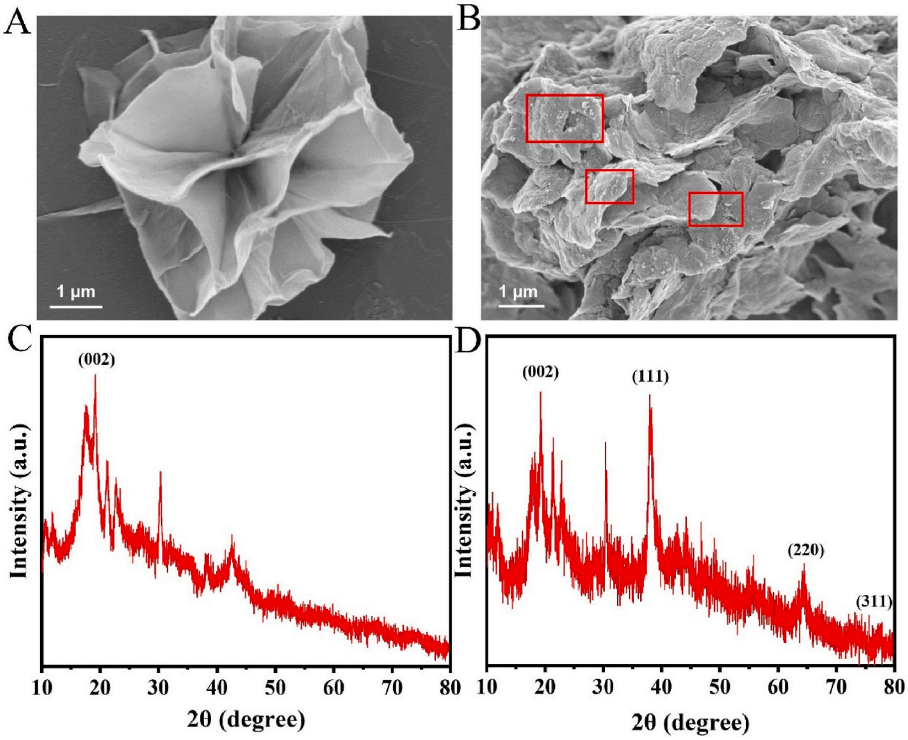

Fig. 2. SEM images of (A) Cu-TCPP MOFs and (B) AgNPs/Cu-TCPP nanozyme. XRD patterns of (C) Cu-TCPP MOFs (D) AgNPs/Cu-TCPP nanozyme.

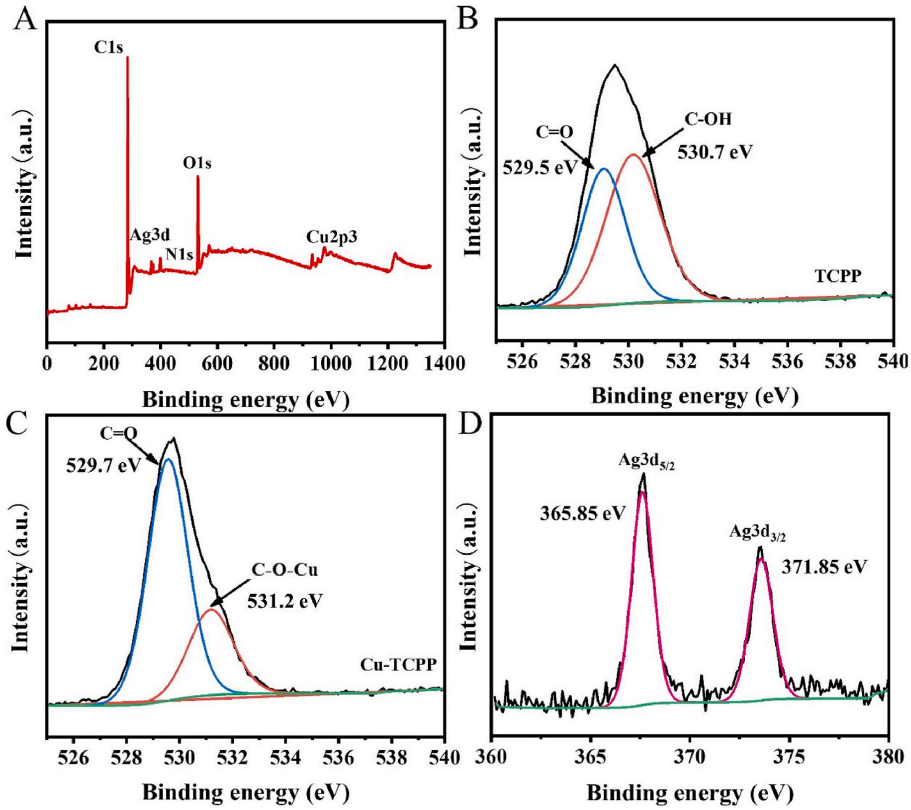

Fig. 3. The full-scan XPS spectra of (A) AgNPs/Cu-TCPP nanozyme. High-resolution XPS spectra of (B) C 1s of TCPP ligands, (C) C 1 s of Cu-TCPP MOFs, (D) Ag 3d of AgNPs/Cu-TCPP nanozyme.

of hydrogen by copper to form C–O–Cu (Lu et al., 2023). This observation suggests the successful coordination of the TCPP ligand with Cu^{2+} (Fig. 3C). After AgNPs were modified on Cu-TCPP, two characteristic peaks of Ag, corresponding to 365.85 eV and 371.85 eV, were observed (Fig. 3D). These experimental results showed that AgNPs/Cu-TCPP was successfully synthesized.

3.3. *Feasibility of the method and mechanism exploration*

To verify the feasibility of the method, UV–vis absorption spectra of TMB in different catalytic systems were shown in Fig. 4A. The substrate solution showed no signal and the solution was colorless. When Cu-TCPP material was added, the solution became light green, and there was a characteristic peak at 650 nm, indicating that Cu-TCPP had typical peroxidase mimetic activity. It can catalyze the formation of colored product (OxTMB) from substrate TMB in the presence of H_2O_2. When AgNPs/Cu-TCPP nanozyme was added into the substrate solution, the solution displayed bright blue, and the absorbance values measured at 650 nm was significantly higher compared to those obtained for Cu-TCPP. This may be due to the AgNPs were uniformly modified on the surface of Cu-TCPP, overcoming the shortcoming that AgNPs tended to aggregate in catalytic reactions (Sabela et al., 2017).

In order to explore the effect of GLY on the peroxidase mimetic catalytic activity of AgNPs/Cu-TCPP nanozyme, the absorption spectra of diverse catalytic systems were measured (Fig. 4B). The substrate solution with GLY showed no signal and the solution was colorless, indicating that GLY has no effect on substrate solution. When AgNPs/Cu-TCPP was added, there was an obvious characteristic peak at 650 nm, which originated from the absorption peak of AgNPs/Cu-TCPP catalyzing H_2O_2 to produce colored product OxTMB. When 50 μmol L^{-1} GLY was added, the absorbance at 650 nm decreased significantly, indicating that GLY inhibited the peroxidase mimetic catalytic activity of AgNPs/Cu-TCPP. In addition, the AgNPs/Cu-TCPP characteristic peak showed a red shift, indicating that GLY may affect the chromophore group of the OxTMB. To explore the influence of the modified AgNPs, the MOF of Cu-TCPP catalyze TMB and H_2O_2 with and without GLY were shown in Fig. S2. Observations indicate that the color and spectral changes in the Cu-TCPP catalyzed TMB reaction solution are not significant, with a low peak value at 650 nm. The difference in absorbance at 410 nm after added of 50 μmol/L GLY is less than 0.4. Therefore, although GLY could similarly inhibit the catalytic activity of Cu-TCPP through binding with Cu^{2+}, its inhibitory effect is not pronounced due to the weak catalytic ability of Cu-TCPP. Consequently, the modification with AgNPs is crucial.

To investigate the potential catalytic mechanism, the electrochemical properties of the materials were characterized. As can be observed in Fig. 4C, the GCE/AgNPs/Cu-TCPP modified electrode exhibited an increase in redox peak currents compared to the bare GCE and GCE/AgNPs. Cyclic voltammetry (CV) curves confirmed that Cu-TCPP can improve the electron transfer rate of AgNPs. Electrochemical impedance spectroscopy (EIS) measurements were conducted on different modified electrodes, the Bode plots was shown in Fig. S3A. The higher slope of the AgNPs/Cu-TCPP-modified GCE at low frequency region indicated that the AgNPs/Cu-TCPP has a faster electron transfer rate compared to the AgNPs. As depicted in Fig. S3B, the AgNPs/Cu-TCPP exhibited a smaller semicircle than the AgNPs, suggesting a reduced charge transfer resistance and enhanced charge transfer capacity. The electrochemical effective area of GCE (Figs. S3C and D) and AgNPs/GCE (Figs. S3E and F) and AgNPs/Cu-TCPP/GCE (Figs. S3G and H) was analyzed at various scanning rates (40–200 mV s^{-1}). Utilizing the CV Randles–Sevcik equation (Pang et al., 2022), the electrochemical effective surface area of the different modified electrodes was determined. After calculation, the AgNPs/Cu-TCPP exhibited higher the electroactive area than AgNPs. According to above analysis, Cu-TCPP might enhance the peroxidase like activity of AgNPs/Cu-TCPP by improving their electrochemical properties.

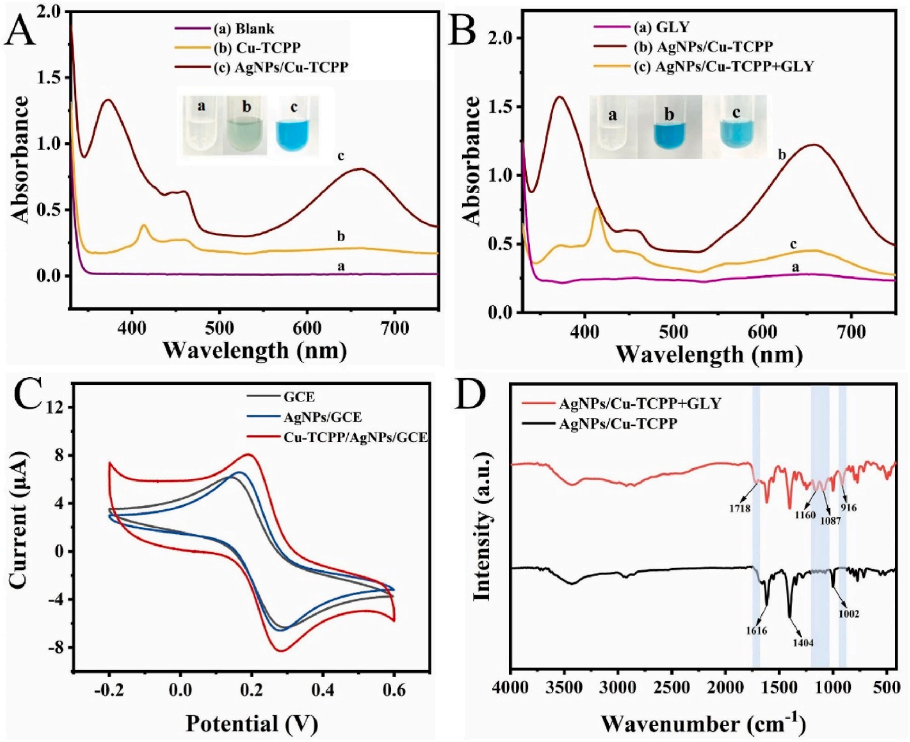

Fig. 4. (A) The UV–vis absorption spectra of TMB + H_2O_2 (a), TMB + H_2O_2 + Cu-TCPP (b) and TMB + H_2O_2 + AgNPs/Cu-TCPP (c). (Inset photography of the corresponding color response under natural light conditions.) (B) The UV–vis absorption spectra of (a) TMB + H_2O_2 + GLY, (b) TMB + H_2O_2 + AgNPs/Cu-TCPP and (c) TMB + H_2O_2 + AgNPs/Cu-TCPP + GLY. (Inset: the corresponding photos). (C) CV curves of different modified electrodes (GCE, AgNPs/GCE and Cu-TCPP/AgNPs/GCE) in $[Fe(CN)_6]^{3-}/[Fe(CN)_6]^{4-}$ (1 mmol L^{-1}, containing 0.2 mol L^{-1} KCl). (D) FTIR spectra of AgNPs/Cu-TCPP and AgNPs/Cu-TCPP + GLY (GLY 400 μmol L^{-1}).

To explore the molecular relationship between AgNPs/Cu-TCPP and GLY, we tested the FTIR spectra of AgNPs/Cu-TCPP before and after the addition of GLY (Fig. 4D). The FTIR spectra of AgNPs/Cu-TCPP displayed distinct absorption peaks, including one at 1002 cm^{-1} that corresponded to the macrocyclic skeleton. Additionally, a peak at approximately 1404 cm^{-1} was ascribed to the stretching vibration of the C═N bond within the pyrrole ring. Meanwhile, a peak at 1607 cm^{-1} signified the vibrational mode of the outer benzene ring's skeleton (Hussain et al., 2021). The same peak was observed in the infrared spectrum of AgNPs/Cu-TCPP after adding GLY, indicating that the addition of GLY did not destroy the covalent structure of the MOF material. However, four new peaks appeared on the spectrum of the AgNPs/Cu-TCPP after adding GLY, the characteristic peaks at 916, 1087 and 1160 cm^{-1}, which were corresponding to the stretching vibration of P–O and P═O of the phosphate group (Wang, Zhu, et al., 2021). The absorption peak at 1718 cm^{-1}, which was part of the carboxylic group-COOH. These results indicated that the GLY can be combined effectively with surface of AgNPs/Cu-TCPP.

According to previous research results (Wan et al., 2022), the strong coordination capacity between divalent copper and GLY has been demonstrated. This might lead to the competitive effect between GLY and AgNPs on the surface of Cu-TCPP. To test this assumption, the Cu 2p XPS spectra of AgNPs/Cu-TCPP before or after GLY treatment was investigated (Fig. 5A and B), the binding energy of AgNPs/Cu-TCPP increased from 953.8 eV to 954.1 (Cu $2p_{1/2}$) and from 933.8 eV to 934.2 (Cu $2p_{3/2}$), which demonstrated that GLY has the stronger ability to chelate Cu-TCPP than AgNPs (Wan et al., 2022). The N 1s XPS spectra of AgNPs/Cu-TCPP before or after GLY treatment was also recorded (Fig. 5C and D), the peak of N 1s can be deconvoluted into two peaks, belonging to N–C═O and C–N/N–H, respectively (Wang, Guo, et al., 2021). After adding the GLY, the proportion of N–C═O increased from 34.1% to 44.4%. This was probably attributed to the formation of amide bonds between Cu-TCPP and GLY. The above results demonstrated that GLY can strongly chelate with Cu-TCPP, competing with AgNPs for active sites on surface of Cu-TCPP, and inhibiting the peroxidase like activity of AgNPs/Cu-TCPP nanozyme.

3.4. Steady-state kinetic analysis of AgNPs/Cu-TCPP nanozyme

In order to explore the steady-state kinetic parameters of AgNPs/Cu-TCPP nanozyme, the steady-state kinetic analysis of AgNPs/Cu-TCPP nanozyme was performed by fixing the concentration of one substrate and changing the concentration of the other substrate. As shown in Fig. 6A and **B**, the reaction rate increased gradually with increasing substrate TMB and H_2O_2 concentrations. When TMB concentration was 2 mmol L^{-1} and H_2O_2 concentration was 80 mmol L^{-1}, the reaction rate reached the maximum. According to Fig. 6C and **D**, steady-state kinetic parameters (including K_m and V_{max}) were calculated according to the Michaelis-Menten equation and Lineweaver-Burk plot. K_m values for the substrates (TMB and H_2O_2) were 1.41 and 3.48, respectively. AgNPs/Cu-TCPP nanozyme showed good catalytic affinity for substrate TMB and H_2O_2.

In the lower concentrations of TMB and H_2O_2, there were two parallel trend lines in the double reciprocal graph, indicating that the reaction catalyzed by AgNPs/Cu-TCPP nanozyme follows ping-pong mechanism. This implied that the first product must leave before binding to the second substrate. When higher concentration of substrate was added, the slope of trend line became smaller, it could be that the reaction is getting saturated.

3.5. Optimization of colorimetric sensing parameters

Considering that the catalytic degree of AgNPs/Cu-TCPP nanozyme was significantly associated with the reaction time, the change of ΔA_{650} with the reaction time was recorded in Fig. S4A. As the catalytic reaction proceeded, ΔA_{650} increased gradually within 20 min, and then plateaued after 20 min. Therefore, in subsequent experiments, the absorbance value at 20 min was recorded.

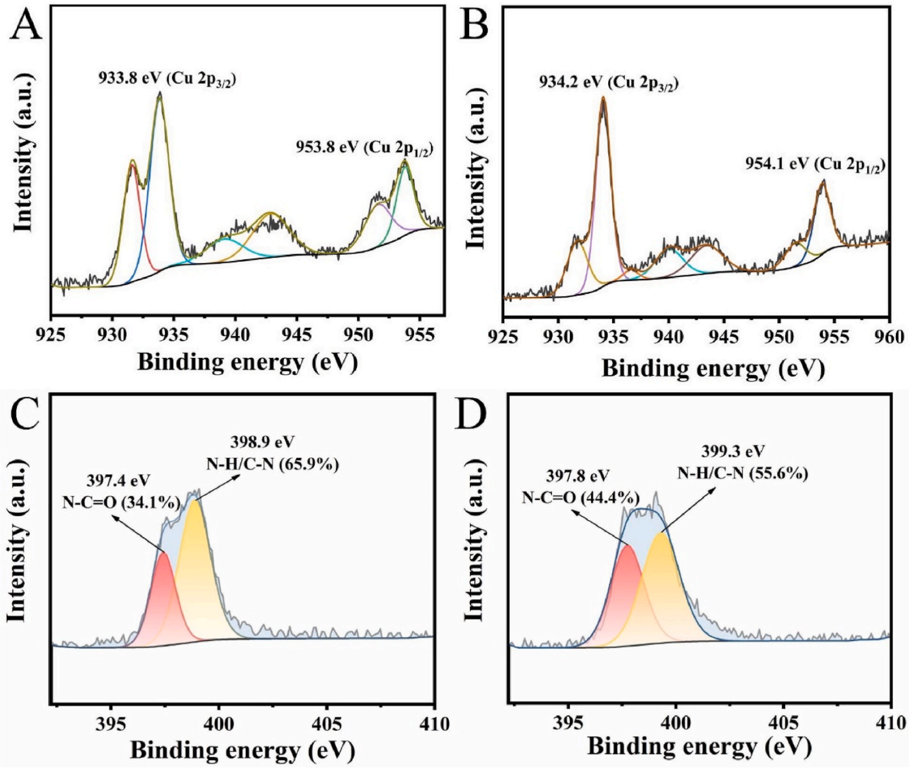

Fig. 5. (A) The Cu 2p (A) and N 1s (C) narrow scan XPS spectra of AgNPs/Cu-TCPP, and the Cu 2p (B) and N 1s (D) narrow scan XPS spectra of AgNPs/Cu-TCPP after adding GLY (GLY 400 μmol L^{-1}).

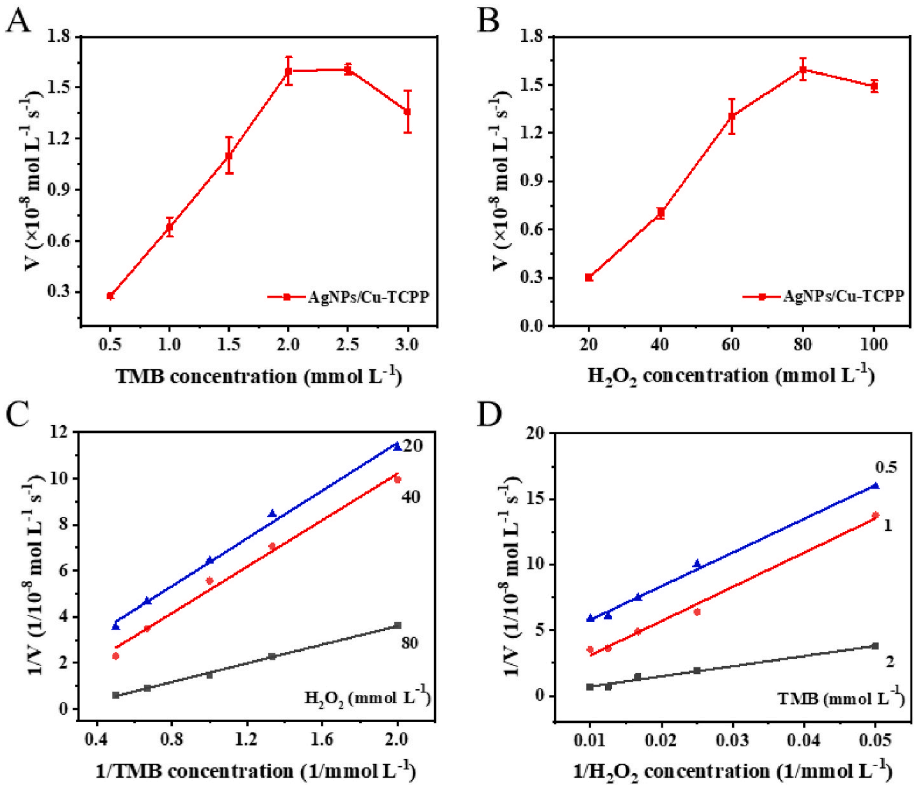

Fig. 6. Steady-state kinetic assays of AgNPs/Cu-TCPP nanozyme. (A, B) The velocity (v) of the reaction was measured using 20 μL AgNPs/Cu-TCPP nanozyme in 0.1 mol L^{-1}ABS buffer (pH 6.0). (C, D) The concentration of H_2O_2 was 80 mmol L^{-1}, TMB was 2 mmol L^{-1} Double-reciprocal plots of activity of AgNPs/Cu-TCPP nanozyme.

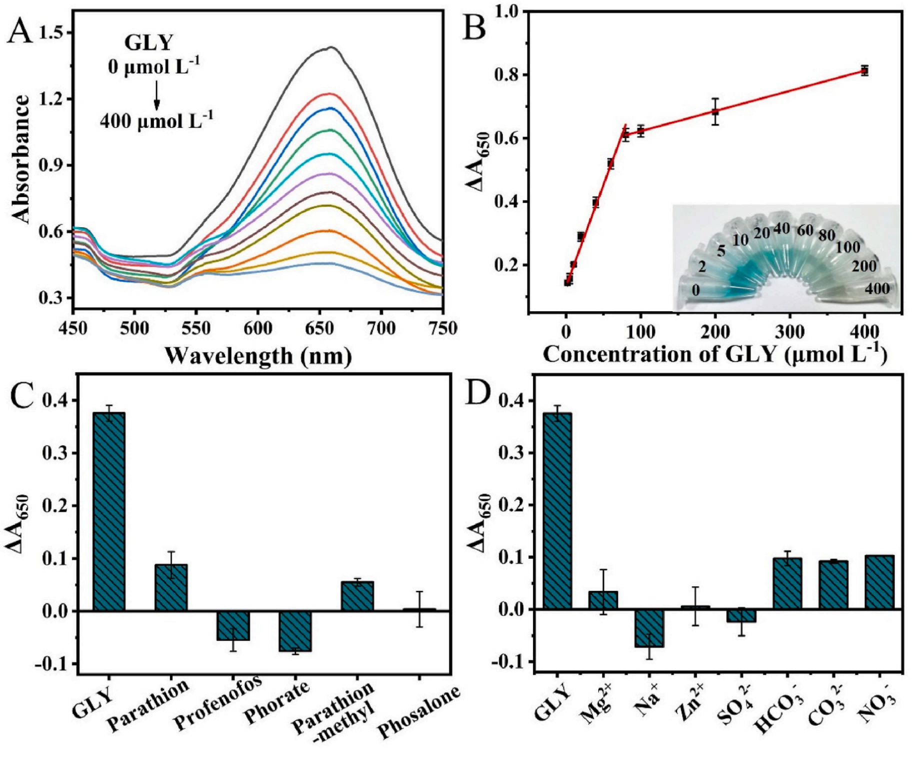

Fig. 7. (A) Absorption spectra and (B) calibration curves with different concentrations of GLY. (C) Selectivity experiment of AgNPs/Cu-TCPP reaction system to GLY and different metal ions (Mg^{2+}, Na^{+}, Zn^{2+}) and acid ions (SO_4^{2-}, HCO_3^-, CO_3^{2-}, NO_3^-). (D) Selectivity of AgNPs/Cu-TCPP to GLY and different kinds of organophosphorus pesticides (parathion, profenofos, phorate, parathion-methyl and phosalone).

Buffer was the principal component of the chemical sensor, and its pH value was important factor for the catalytic ability of the nanozyme (Fig. S4B). As the pH value was increased, ΔA_{650} increased gradually until it reached the maximum value at pH 6. When the pH value decreased or further increased, the signal decreased, which may be due to the formation of hydroxyl radicals was suppressed in an overly acidic or alkaline environment (Wu et al., 2022). Therefore, a buffer of pH 6 was selected.

Concentration of TMB was directly related to the color change of the sensor solution, the influence was also shown in Fig. S4C. As TMB concentration increasing, the signal increased rapidly. When TMB concentration was 2 mmol L^{-1}, the signal value reached the maximum. Therefore, 2 mmol L^{-1} TMB was selected for colorimetric sensing of GLY.

H_2O_2 can be catalyzed by AgNPs/Cu-TCPP to generate hydroxyl radicals, thus affecting the color change of solution. The influence of H_2O_2 concentration was shown in Fig. S4D. As H_2O_2 concentration increasing, the signal increased gradually and reached the peak value at 80 mmol L^{-1}. Therefore, 80 mmol L^{-1} H_2O_2 was selected for GLY colorimetric sensing.

3.6. Method validation

A variety of GLY concentrations were used in the catalytic reaction system to determine the sensitivity of the colorimetric sensing method based on AgNPs/Cu-TCPP nanozyme. The absorption signal was plotted in Fig. 7A, revealing a distinct trend. As the concentration of GLY rose, the absorbance demonstrated a decline trend. Specifically, within the concentration range of 2–400 μmol L^{-1}, the ΔA_{650} value exhibited a gradual decrease as the GLY concentration increased, displaying a distinct two-segment piecewise linear trend. Notably, a linear correlation was observed between ΔA_{650} and GLY concentration from 2 to 80 μmol L^{-1}, with the linear equation being $\Delta A_{650} = 0.00636C_{GLY}+0.13376$ ($R^2 = 0.993$). This linear relationship persisted in the concentration range of 80–400 μmol L^{-1}, with the linear equation being $\Delta A_{650} = 0.00064C_{GLY}+0.55871$ ($R^2 = 0.999$). In Fig. 7B, as the GLY concentration increased, the color of the reaction system gradually changed from aquamarine blue to colorless, which realized the visual detection of GLY, and the pesticide residues were able to putatively identify by naked eyes. The nanozyme colorimetric sensing method boasts a limit of detection (LOD) was 0.67 μmol L^{-1} (S/N = 3), which can make colorimetric sensor useful for monitoring the concentration of GLY in actual samples. Meanwhile, the naked eye can judge whether pesticide residues exceed the standard, which provides a new method for rapid detection of GLY.

To investigate the inhibition of other pesticides on AgNPs/Cu-TCPP nanozyme. The potentially competitive organophosphorus pesticides (phosalone, profenofos, parathion, parathion-methyl and phorate) containing 10 times the concentration of GLY were added to the reaction system. The results were presented in Fig. 6C, other competitive pesticides had little interference on the detection results, which further verified that the constructed colorimetric sensing method has good selectivity for GLY. To verify the selectivity of the method, a series of interfering ions were added to the reaction system containing TMB and H_2O_2, including common metal ions (Mg^{2+}, Na^{+}, Zn^{2+}) and general acid ions (SO_4^{2-}, HCO_3^{-}, CO_3^{2-}, NO_3^{-}). As showed in Fig. 7D, there is no obvious interference of these coexisting substances.

The colorimetric GLY sensing method constructed in this paper was compared with other methods, and Table 1 showed the obtained values. It can be found that the colorimetric sensing method based on AgNPs/Cu-TCPP nanozyme demonstrates a broadened linear range and a reduced LOD compared to previously documented methods. Furthermore, it boasts the advantages of visibility, straightforward operation, and prompt response. The AgNPs/Cu-TCPP colorimetric sensing system in food and agricultural products for real-time visual monitoring has broad prospects.

Table 1
Comparison with previously reported colorimetric methods for GLY sensing.

Sensing materials	Linear range (μmol L^{-1})	LOD (μmol L^{-1})	Application	References
MoS_2 Nanoflake	2.37–11.83	0.51	Environmental water	Chen et al. (2017)
CS_2	21.89–47.33	6.51	Soil, wheat, water samples	Jan et al. (2009)
Cu(II)-PV	2.5–60	2.66	Tap water	Yadav and Zelder (2021)
AgNPs/Cu-TCPP	2–400	0.67	Drinking water, cucumber	This paper

3.7. Determination of GLY in real samples

To investigate the applicability of the colorimetric sensing system in real samples, the AgNPs/Cu-TCPP nanozyme sensor was employed to determinate the concentration of GLY in drinking water and cucumber. The results showed that GLY was not found in different brands of drinking water and cucumber. The standard addition method was used to carry out recovery experiments. 5, 10 μmol L^{-1} GLY was added to the real samples, respectively. The accuracy of the developed sensing approach was assessed. Table 2 presents the findings of the standard addition experiments. The recovery rates of actual samples ranged from 98.3% to 103.5%, with a relative standard deviation (RSD) below 5.9%.

4. Conclusion

In summary, a AgNPs/Cu-TCPP nanozyme was synthesized and it can catalyze the oxidation of TMB and produce blue OxTMB in the presence of H_2O_2. Moreover, the catalytic performance of the nanozyme also can be specifically blocked by glyphosate. The catalytic efficiency and reaction kinetic of AgNPs/Cu-TCPP nanozyme were similar to those of natural enzymes, and followed the typical Michaelis-Menten curve. The GLY could bind specifically to AgNPs/Cu-TCPP with a chelating interaction, thereby competing with AgNPs for active sites on surface of Cu-TCPP and inhibiting the peroxidase mimetic activity of AgNPs/Cu-TCPP. According to this mechanism, a novel colorimetric sensor for detection of GLY by absorbance or just by naked eye was developed. This colorimetric sensing method holds potential for the development of high-performance glyphosate (GLY) sensors that can directly detect organophosphates (OPs) without reliance on natural enzymes. Moreover, the method's distinct and easily discernible color changes, coupled with

Table 2
Detection of GLY in food samples.

Samples	Added (μmol L^{-1})	Found (μmol L^{-1})	Recovery (%)	RSD(n = 3) (%)
Drinking water 1	0	ND[1]	–	–
	5	4.86	99.5	4.9
	10	10.69	102.2	2.4
Drinking water 2	0	ND	–	–
	5	5.02	100.1	4.9
	10	10.66	102.2	2.9
Drinking water 3	0	ND	–	–
	5	4.81	99.3	5.1
	10	10.52	101.7	3.7
Cucumber	0	ND	–	–
	5	4.54	98.3	5.3
	10	11.09	103.5	5.9

ND[1]: Not detected.

a portable spectrophotometer, facilitate qualitative and quantitative detection in field settings.

CRediT authorship contribution statement

Li-Hong Yu: Writing – original draft, Methodology, Investigation, Formal analysis, Conceptualization. **Rui Jiang:** Validation, Methodology, Formal analysis. **Cheng-Lin Yang:** Methodology, Formal analysis, Conceptualization. **Yue-Hong Pang:** Writing – review & editing, Methodology, Conceptualization. **Xiao-Fang Shen:** Writing – review & editing, Resources, Project administration, Funding acquisition, Conceptualization.

Declaration of competing interest

The authors declare that they have no known competing financial interests or personal relationships that could have appeared to influence the work reported in this paper.

Data availability

Data will be made available on request.

Acknowledgments

This work was supported by the National Natural Science Foundation of China (22076067).

Appendix A. Supplementary data

Supplementary data to this article can be found online at https://doi.org/10.1016/j.fbio.2024.104577.

References

Berry, C. (2020). Glyphosate and cancer: The importance of the whole picture. *Pest Management Science, 76*(9), 2874–2877.

Chang, J., Yu, L., Hou, T., Hu, R., & Li, F. (2023). Direct and specific detection of glyphosate using a phosphatase-like nanozyme-mediated chemiluminescence strategy. *Analytical Chemistry, 95*(9), 4479–4485.

Chen, Q., Chen, H., Li, Z., Pang, J., Lin, T., Guo, L., & Fu, F. (2017). Colorimetric sensing of glyphosate in environmental water based on peroxidase mimetic activity of MoS_2 nanosheets. *Journal of Nanoscience and Nanotechnology, 17*(8), 5730–5734.

Chen, H., Qiu, Q., Sharif, S., Ying, S., Wang, Y., & Ying, Y. (2018). Solution-phase synthesis of platinum nanoparticle-decorated metal-organic framework hybrid nanomaterials as biomimetic nanoenzymes for biosensing applications. *ACS Applied Materials & Interfaces, 10*(28), 24108–24115.

Coutinho, C. F. B., Silva, M. O., Machado, S. A. S., & Mazo, L. H. (2007). Influence of glyphosate on the copper dissolution in phosphate buffer. *Applied Surface Science, 253*(6), 3270–3275.

Dallegrave, E., Mantese, F. D., Coelho, R. S., Pereira, J. D., Dalsenter, P. R., & Langeloh, A. (2003). The teratogenic potential of the herbicide glyphosate-roundup in wistar rats. *Toxicology Letters, 142*(1–2), 45–52.

De Almeida, L. K. S., Chigome, S., Torto, N., Frost, C. L., & Pletschke, B. I. (2015). A novel colorimetric sensor strip for the detection of glyphosate in water. *Sensors and Actuators B: Chemical, 206*, 357–363.

Duke, S. O. (2018). The history and current status of glyphosate. *Pest Management Science, 74*(5), 1027–1034.

Farhadi, S., Riahi-Madvar, A., Sargazi, G., & Mortazavi, M. (2021). Immobilization of Lepidium draba peroxidase on a novel Zn-MOF nanostructure. *International Journal of Biological Macromolecules, 173*, 366–378.

Gao, L., Zhuang, J., Nie, L., Zhang, J., Zhang, Y., Gu, N., Wang, T., Feng, G., Yang, D., Perrett, S., & Yan, X. (2007). Intrinsic peroxidase-like activity of ferromagnetic nanoparticles. *Nature Nanotechnology, 2*(9), 577–583.

Graf, H. G., Biebl, S. M., Muller, L., Breitenstein, C., & Huhn, C. (2022). Capillary electrophoresis applied for the determination of acidity constants and limiting electrophoretic mobilities of ionizable herbicides including glyphosate and its metabolites and for their simultaneous separation. *Journal of Separation Science, 45*(5), 1128–1139.

Guyton, K. Z., Loomis, D., Grosse, Y., El Ghissassi, F., Benbrahim-Tallaa, L., Guha, N., Scoccianti, C., Mattock, H., & Straif, K. (2015). Carcinogenicity of tetrachlorvinphos, parathion, malathion, diazinon, and glyphosate. *Lancet Oncology, 16*(5), 490–491.

Hu, Z., Tao, C.-a., Liu, H., Zou, X., Zhu, H., & Wang, J. (2014). Fabrication of an NH2-MIL-88B photonic film for naked-eye sensing of organic vapors. *Journal of Materials Chemistry A, 2*(34).

Huang, Y., Zhao, M., Han, S., Lai, Z., Yang, J., Tan, C., Ma, Q., Lu, Q., Chen, J., Zhang, X., Zhang, Z., Li, B., Chen, B., Zong, Y., & Zhang, H. (2017). Growth of Au Nanoparticles on 2D metalloporphyrinic metal-organic framework nanosheets used as biomimetic catalysts for cascade reactions. *Advanced Materials, 29*(32).

Hussain, S., Deng, Z., Khan, A., Li, P., Li, Z., Fang, Z., Wan, X., & Peng, X. (2021). Photothermal responsive ultrathin Cu-TCPP nanosheets/sulfonated polystyrene nanocomposite photo-switch proton conducting membranes. *Journal of Membrane Science, 620*.

Jan, M. R., Shah, J., Muhammad, M., & Ara, B. (2009). Glyphosate herbicide residue determination in samples of environmental importance using spectrophotometric method. *Journal of Hazardous Materials, 169*(1–3), 742–745.

Kirandeep, Husain, A., Kumar Kharwar, A., Kataria, R., & Kumar, G. (2019). Co(II)-based metal–organic frameworks and their application in gas sorption and solvatochromism. *Crystal Growth & Design, 19*(3), 1640–1648.

Li, G.-B., Li, L., Liu, J.-M., Yang, T., & Su, C.-Y. (2013). A CdSO4-type 3D metal–organic framework showing coordination dynamics on Cu^{2+} axial sites: Vapochromic response and guest sorption selectivity. *Crystal Growth & Design, 13*(4), 1518–1525.

Li, D., Zhang, S., Feng, X., Yang, H., Nie, F., & Zhang, W. (2019). A novel peroxidase mimetic Co-MOF enhanced luminol chemiluminescence and its application in glucose sensing. *Sensors and Actuators B: Chemical, 296*.

Liu, M., Zhang, S., Wang, Y., Liu, J., Hu, W., & Lu, X. (2022). Hexavalent chromium as a smart switch for peroxidase-like activity regulation via the surface electronic redistribution of silver nanoparticles anchored on carbon spheres. *Analytical Chemistry, 94*(3), 1669–1677.

Liu, T., Zhou, M., Pu, Y., Liu, L., Li, F., Li, M., & Zhang, M. (2021). Silver nanoparticle-functionalized 3D flower-like copper (II)-porphyrin framework nanocomposites as signal enhancers for fabricating a sensitive glutathione electrochemical sensor. *Sensors and Actuators B: Chemical, 342*.

Lu, M., Dong, A., Li, X., Liu, X., Zhang, Z., Tian, T., & Jing, L. (2023). The synthesis of Cu-TCPP MOF/g-C_3N_4 heterojunctions as efficient photocatalysts for hydrogen generation. *New Journal of Chemistry, 47*(44), 20336–20343.

Ma, J., Bai, W., & Zheng, J. (2019). Non-enzymatic electrochemical hydrogen peroxide sensing using a nanocomposite prepared from silver nanoparticles and copper (II)-porphyrin derived metal-organic framework nanosheets. *Mikrochimica Acta, 186*(7), 482.

Nova, P., Calheiros, C. S. C., & Silva, M. (2020). Glyphosate in Portuguese adults - a pilot study. *Environmental Toxicology and Pharmacology, 80*.

Pang, Y. H., Wang, Y. Y., Shen, X. F., & Qiao, J. Y. (2022). Covalent organic framework modified carbon cloth for ratiometric electrochemical sensing of bisphenol A and S. *Mikrochimica Acta, 189*(5), 189.

Sabela, M., Balme, S., Bechelany, M., Janot, J. M., & Bisetty, K. (2017). A review of gold and silver nanoparticle-based colorimetric sensing assays. *Advanced Engineering Materials, 19*(12).

Wan, C. Q., Pang, Y. H., Feng, Y. W., & Shen, X. F. (2022). A ratio fluorescence sensor based on rhodamine B embedded metal-organic framework for glyphosate detection in agri-food products. *Food Chemistry, 394*, Article 133446.

Wang, Y., Guo, Y., Li, H., Zhou, R., Yu, J., Hou, H., Yin, W., & Chi, R. (2021). Sequential recycle of valuable phosphorus compounds of glyphosine, glyphosate, and phosphorous acid from glyphosate mother liquor by D301 resin through sorbent dosage control. *Journal of Environmental Chemical Engineering, 9*(6).

Wang, L., Hu, Z., Wu, S., Pan, J., Xu, X., & Niu, X. (2020). A peroxidase-mimicking Zr-based MOF colorimetric sensing array to quantify and discriminate phosphorylated proteins. *Analytica Chimica Acta, 1121*, 26–34.

Wang, Z., Zhu, J., Xu, S., Zhang, Y., & Van der Bruggen, B. (2021). Graphene-like MOF nanosheets stabilize graphene oxide membranes enabling selective molecular sieving. *Journal of Membrane Science, 633*.

Wei, X., Pan, Y., Zhang, Z., Cui, J., Yin, R., Li, H., Qin, J., Li, A. J., & Qiu, R. (2024). Biomonitoring of glyphosate and aminomethylphosphonic acid: Current insights and future perspectives. *Journal of Hazardous Materials, 463*, Article 132814.

Wu, Z., Hu, Y., Pan, X., Tang, Y., Dai, Y., & Wu, Y. (2022). A liquid colorimetric chemosensor for ultrasensitive detection of glyphosate residues in vegetables using a metal oxide with intrinsic peroxidase catalytic activity. *Food Additives & Contaminants Part A-Chemistry Analysis Control Exposure & Risk Assessment, 39*(4), 710–723.

Xu, B., Wang, H., Wang, W., Gao, L., Li, S., Pan, X., Wang, H., Yang, H., Meng, X., Wu, Q., Zheng, L., Chen, S., Shi, X., Fan, K., Yan, X., & Liu, H. (2019). A Single-atom nanozyme for wound disinfection applications. *Angewandte Chemie-international Edition, 58*(15), 4911–4916.

Yadav, P., & Zelder, F. (2021). Detection of glyphosate with a copper(II)-pyrocatechol violet based GlyPKit. *Analytical Methods, 13*(38), 4354–4360.

Yoshioka, N., Asano, M., Kuse, A., Mitsuhashi, T., Nagasaki, Y., & Ueno, Y. (2011). Rapid determination of glyphosate, glufosinate, bialaphos, and their major metabolites in serum by liquid chromatography-tandem mass spectrometry using hydrophilic interaction chromatography. *Journal of Chromatography A, 1218*(23), 3675–3680.

Zhang, T., Xing, Y., Song, Y., Gu, Y., Yan, X., Lu, N., Liu, H., Xu, Z., Xu, H., Zhang, Z., & Yang, M. (2019). AuPt/MOF-graphene: A synergistic catalyst with surprisingly high peroxidase-like activity and its application for H_2O_2 detection. *Analytical Chemistry, 91*(16), 10589–10595.